PAPER

Advancing Non-Cuff Hypertension Detection: Leveraging 1D Convolutional Neural Network and Time Domain Physiological Signals

Nuryani Nuryani[1](✉),
Trio Pambudi Utomo[1],
Nurhasan Agung Prabowo[2],
Aripriharta[3], Muhammad
Yazid[4], Mohtar Yunianto[1]

[1]Department of Physics,
University of Sebelas Maret,
Suarakrta, Indonesia

[2]Faculty of Medicine,
University of Sebelas Maret,
Surakarta, Indonesia

[3]Electrical Engineering,
Universitas Negeri Malang,
Malang, Indonesia

[4]Biomedical Engineering,
Institut Teknologi
Sepuluh Nopember,
Surabaya, Indonesia

nuryani@mipa.uns.ac.id

ABSTRACT

Timely identification of hypertension (HT) is crucial for effectively managing and reducing the potential health consequences, including cardiovascular events such as heart attacks and strokes, as well as the development of kidney disease. Traditional cuff-based devices often discourage regular monitoring because they cause discomfort. Furthermore, the lack of symptoms in HT complicates the early detection of this condition. To address these challenges, our study employs a non-cuff methodology that utilizes unprocessed electrocardiogram (ECG) and photoplethysmogram (PPG) signals. We utilize a customized approach to enhance the features of a one-dimensional convolutional neural network (CNN) specifically tailored to optimize time-series data. In contrast to previous research, our methodology avoids the need for complex signal extraction or transformation techniques. The main goal is to identify the optimal input signals and fine-tune the critical hyperparameters of CNNs. The clinical data underwent analysis, which revealed that the use of an integrated ECG and PPG approach resulted in the highest level of accuracy for detection. Notably, the F1 score achieved an impressive value of 98.88%. When evaluated separately, ECG outperformed PPG. Our study contributes to the advancement of the field by introducing a new approach that combines comfort and high accuracy in the early detection of HT. This method is practical and ensures a patient-friendly experience.

KEYWORDS
hypertension (HT) detection, electrocardiogram (ECG), photoplethysmogram (PPG), convolutional neural network (CNN), non-cuff methods

1   INTRODUCTION

High blood pressure, or hypertension (HT), is a significant global health issue. It is associated with conditions such as strokes [1] and diabetes [2] and is acknowledged

as a significant risk factor for sudden cardiac death [3]. Between 1990 and 2019, there was a significant increase in the prevalence of HT among individuals aged 30–79 years. This increase resulted in the numbers rising from 331 million women and 317 million men in 1990 to 626 million women and 652 million men in 2019. Managing this health condition is demanding and expensive, and one of its main challenges is early diagnosis [4]. HT is often referred to as the "silent killer" because it typically does not show symptoms until it reaches an advanced stage, making it particularly challenging to detect [5]. Currently, the standard method for diagnosing and monitoring HT involves using a sphygmomanometer [6], which classifies patients into four stages of HT: normal, prehypertension (PHT), stage 1 HT, and stage 2 HT [7]. These stages are determined by systolic and diastolic blood pressure.

The challenge is that cuff-based monitoring systems only offer a single snapshot of blood pressure, requiring multiple readings and averaging to obtain a dependable value. Furthermore, they may cause discomfort as a result of arterial compression [8]. Additionally, self-measurements using cuff-based devices can lead to inaccurate diagnoses if proper methodologies are not followed [9]. To meet the need for a more refined and minimally invasive method of monitoring HT, several technologies have been developed, including the use of photoplethysmogram (PPG) and electrocardiogram (ECG) waveforms [10]. Various techniques have been employed, such as calculating the pulse arrival time (PAT) obtained from both ECG and PPG waveforms. Another technique uses parameters solely from PPG [11]. These ECG and PPG characteristics are then utilized as inputs for regression or classification machine learning techniques [12] or deep learning techniques [13] to monitor or detect HT. Another approach uses a continuous wavelet transform ballistocardiogram (BCG) in conjunction with deep learning [14]. Furthermore, socio-demographic and clinical variables, such as age, gender, and body mass index (BMI), have been utilized in the development of machine learning-based systems for detecting HT [15].

Nevertheless, the journey is marked by several challenges that require careful consideration when developing blood pressure estimation systems or strategies for assessing HT risk. Firstly, extensive research has focused on developing systems for detecting HT that utilize ECG and PPG signals. These systems use feature extraction techniques to identify ECG and PPG signal parameters. The extraction of these signals involves numerous parameters and leads to a wide range of potential combinations. Each unique combination requires individual testing to determine the best performance, resulting in long experimental durations.

Furthermore, the extraction process may necessitate high-quality waveforms, a high sampling rate, and precise sampling accuracy to acquire pertinent signal parameters. Additionally, further research is needed to thoroughly compare detection systems that solely utilize ECG signals, PPG signals, or a combination of both. The scarcity of research on this aspect is evident. A comparative analysis like this has the potential to provide valuable insights, shedding light on the best choice of signals for achieving improved performance levels. Finally, socio-demographic and clinical variables, such as age, gender, and body mass index, have been utilized in the development of machine learning-based systems for high blood pressure risk stratification. However, this methodology is less practical when considering an automated detection approach.

Following the introduction, this paper presents a systematic exploration of our research efforts. Initially, we highlight our "innovations and breakthroughs," emphasizing the new perspectives and contributions we bring to the academic landscape. To position our work within a broader scholarly framework, the "related works"

section explores existing literature. We then outline our investigative approach in the 'methods' section, providing readers with a clear view of our research design and procedures. Our "results" section presents the empirical evidence and outcomes of our investigation. In the "discussion," we interpret and contextualize these results, drawing connections to existing knowledge while highlighting potential ramifications. The "limitations" segment offers a candid reflection on possible constraints and shortcomings. In conclusion, we encapsulate the essence, implications, and prospects of our study.

2 INNOVATIONS AND BREAKTHROUGHS

This paper introduces an approach for identifying HT using direct input from ECG and PPG signals without the need for feature extraction. One notable benefit of this approach is the prevention of potential data loss during the extraction phase. By avoiding the process of feature extraction, the original data retains its richness and integrity. Moreover, eliminating extraction steps improves the computational process, thus increasing efficiency. The streamlined methodology used in this study enhances computational speeds. It enables the development of real-time applications, making it a highly suitable option for implementing advanced tools such as wearable devices and remote patient monitoring systems.

This study conducts a thorough analysis to explore the different roles of ECG and PPG. The analysis covers three distinct areas: the individual capabilities of ECG and PPG and their combined effectiveness when integrated. The ECG plays a crucial role in identifying indicators of HT due to its ability to provide information about the heart's electrical activity. Following this, the focus shifts to PPG, emphasizing its ability to detect changes in blood volume and provide important hemodynamic insights. Furthermore, integrating ECG and PPG signals can enhance diagnostic accuracy by comprehensively assessing the body's physiological indicators.

Furthermore, the research delves into an extensive investigation of various CNN (convolutional neural network) architectures [16–18]. The main objective is to investigate different configurations of CNNs, including parameters such as stride, kernel size, and filter selection. This study aims to determine whether specific designs demonstrate improved accuracy in identifying HT. The current comprehensive assessment of CNN architectures is grounded in the hypothesis that custom-designed neural networks could enhance the capacity to accurately represent the complex patterns within HT data.

Finally, the study conducts a series of experiments across three trials to comprehensively detect HT. In Trial A, the study compares individuals with normal and prehypertensive blood pressure, revealing early indicators of HT. Normal vs. HT (Trial B): This segment differentiates between normal and hypertensive blood pressure readings. Normal blood pressure vs. PHT. HT (Trial C): This trial offers a comprehensive analysis of blood pressure progression across normotensive, prehypertensive, and hypertensive cohorts, providing a thorough understanding of the condition.

Essentially, this paper is based on several fundamental contributions. First, it introduces the direct integration of ECG and PPG signals into the HT detection paradigm, effectively negating the need for feature extraction. Second, the article provides a detailed exploration of the specific roles of ECG and PPG signals in the detection mechanism. Third, various CNN architectures are thoroughly analyzed to enhance detection accuracy. Finally, the research presents a systematic series of experiments.

Each of these experiments consists of separate trials that cover a wide range of blood pressure classifications.

3   RELATED WORKS

In the context of past research endeavors, various models were conceived that harnessed the power of machine learning [19, 20] and deep learning [21] techniques to refine the process of HT detection. These models demonstrated a remarkable capacity to utilize clinical data and physiological waveforms as foundational inputs. To streamline this procedure, the models underwent training utilizing a diverse range of variables, encompassing, though not exclusively, age, body mass index, gender, and heart rate. Furthermore, they accommodated, using PPG and ECG waveforms, precisely the characteristics extracted through a comprehensive suite of analytical techniques. As previously explained in research, these techniques include time analysis, frequency analysis, time-frequency analysis, and chaotic analysis. A notable aspect of these studies was the thorough investigation of morphological features extracted from ECG and PPG signals. This approach provided a comprehensive overview of the diverse strategies deployed for detecting hypertension.

In the realm of investigating the correlation between ECG and blood pressure, a study emphasized that alterations in ECG patterns associated with HT gradually appear and manifest, even in healthy young individuals with normal to slightly elevated blood pressure levels. These changes were significantly linked to various physiological shifts, including increased ventricular rate, enlarged atrial surface area, extended ventricular activation time, heightened ventricular hypertrophy indices, and noticeable alterations in ventricular repolarization detected through a standard twelve-lead electrocardiogram. This indicates a gradual development of cardiovascular adjustments in individuals who do not have diagnosed HT but have blood pressure levels within the upper range of normal [22].

The investigation revealed a significant relationship between arterial pressure (specifically systolic and mean) and pulse wave velocity derived from PPG during the post-exercise recovery phase following a cycling test. This sheds light on the connection between PPG-derived metrics and blood pressure dynamics. The significant correlation observed strongly indicates that changes in arterial blood pressure are intricately linked to alterations in pulse wave velocity. Furthermore, the study found consistent correlations across various vascular sites, regardless of the specific location for measuring pulse wave velocity. This confirms a consistent relationship between arterial blood pressure and pulse wave velocity across diverse vascular locations. These findings emphasize a strong connection between arterial blood pressure and pulse wave velocity [23].

In 2022, a research study introduced a machine-learning-based system for identifying HT [19]. The method utilized a combination of PPG features and clinical data as input variables. Five machine learning algorithms were utilized, specifically support vector machines (SVM), logistic regression (LR), linear discriminant analysis (LDA), k-nearest neighbors (KNN), and decision trees. The study utilized a set of nineteen PPG characteristics obtained through the application of the wavelet scattering transform method. The clinical data included age, gender, body mass index (BMI), heart rate, height, and weight. The peak of success using this approach was indicated by a 76.00% F1 score. The optimal result emerged when only PPG features were used. The integration of PPG and clinical data led to a decrease in the F1 score to 72.34%. Furthermore, a more significant decline to 69.57% was observed when only clinical

data was utilized. The study results indicate that incorporating clinical data, such as age and BMI, did not improve the overall performance of the system. From the standpoint of machine learning methodologies, the investigation encountered no obstacles. The parameters of the machine learning models were skillfully adjusted to achieve the most favorable detection outcome.

In 2021, a study reported on research into a HT detection system that utilized PPG features and machine learning techniques [24]. PPG features were obtained by extracting features from PPG signals. However, these PPG signals had to undergo a two-step derivative process to generate the first and second derivatives. Furthermore, after obtaining these derivatives, additional steps were necessary to identify multiple reference points in both the original and derivative signals for extracting parameter values. Determining fiducial points was susceptible to errors that could result in inaccuracies. Moreover, this method utilized complex algorithmic processing, including Ceemdan and Wavelet algorithms, to generate highly accurate PPG signals. Complex algorithms often require increased computing resources. Compared to simpler algorithms, these algorithms may require more processing power, memory, and time to execute.

In 2020, [15] introduced a method for developing a HT classification system. This method utilized clinical data that included gender, race, BMI, age, smoking habits, kidney disease, and diabetes. The study utilized an artificial neural network with back-propagation as the classification technique. The dataset used for analysis comprised a substantial 24,434 records from the National Health and Nutrition Examination Survey spanning 2007 to 2016. The study findings showed a sensitivity rate of 40%, a specificity rate of 87%, a precision rate of 57.8%, and an AUC (area under the curve) value of 0.77. It is worth noting that, despite the extensive dataset, the performance achieved through this approach did not reach the desired level of excellence.

Researchers have explored various methodologies within the broader context of detecting and classifying HT. These techniques include machine learning, or deep learning, integrating ECG and PPG features, as well as intricate signal processing algorithms. Furthermore, clinical data, including gender, race, BMI, age, smoking habits, kidney disease, and diabetes, has been employed. These studies have undoubtedly provided valuable insights into the complexities and possibilities of detecting and classifying HT. However, there is a persistent need for further research and innovation to overcome these challenges and establish more robust and dependable HT detection systems.

4   METHODS

The general methodology for this study on HT detection, which involves the use of ECG and PPG signals along with CNN learning, is outlined in Figure 1. We began by preparing the ECG and PPG signals, as well as the correlated atrial blood pressure (ABP). Following this, we identified the peaks of the QRS complex in the ECG signals and the pulse peaks in the PPG signals. To prepare the input for the CNN, we gathered 50 ECG samples from both sides of each identified QRS peak and 50 PPG samples from both sides of each identified pulse peak. We then proceeded to the training, validation, and testing stages of the CNN. We experimented with different kernel sizes, strides, and filters during this phase to optimize the network's performance. Ultimately, we developed an optimized CNN model specifically designed for detecting HT. The methodology's details are further described in the subsequent sections.
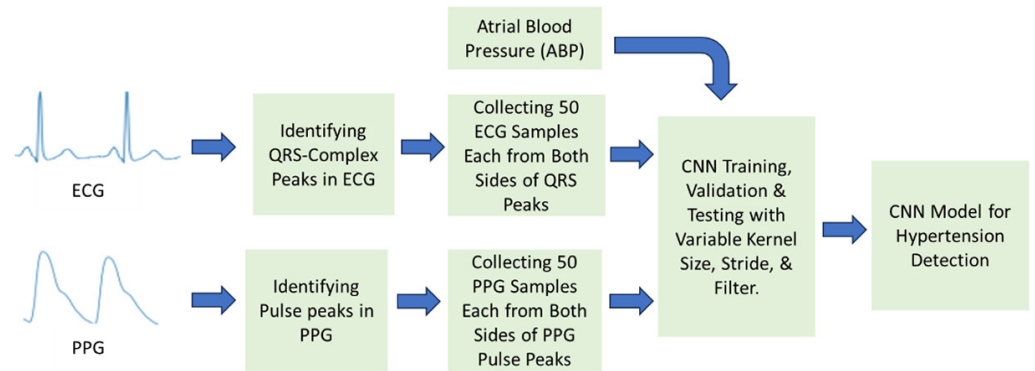
Fig. 1. Workflow for hypertension detection using CNN with the inputs of ECG and PPG

4.1 Data collection and categorization

This study gathered data from the multiparameter intelligent monitoring in intensive care (MIMIC) database [25, 26], which included measurements of PPG, ECG, and arterial blood pressure (ABP). The primary objective was to distinguish between different blood pressure levels, specifically normotension (NT), PHT, and HT, by utilizing data from PPG and ECG signals. The blood pressure categories were determined based on the ambulatory blood pressure (ABP) data and followed the guidelines outlined in the JNC 7 report [27]. The experimental design of this study involved binary classification techniques, resulting in two distinct class labels. The study consisted of three trials: Trial A, Trial B, and Trial C. In Trial A, the classification focused on NT vs. PHT; Trial B compared NT vs. HT; and Trial C examined NT-PHT vs. HT classifications.

To ensure the reliability and accuracy of the data, we conducted a comprehensive examination of the database, specifically addressing potential errors in data matching and alignment in specific recordings [28]. During this screening process, we excluded records with biphasic pulses, missing peaks, or instances without a signal (sensor-off). We identified 121 records with high-quality signals and selected 120 seconds of data from each record for further analysis, as described in reference [28]. Our dataset consisted of 17,534 records, categorized as 6,129 for normotension, 4,966 for PHT, and 6,397 for hypertension. The ECG and PPG examples for three distinct classes are shown in Figures 2 and 3, respectively.
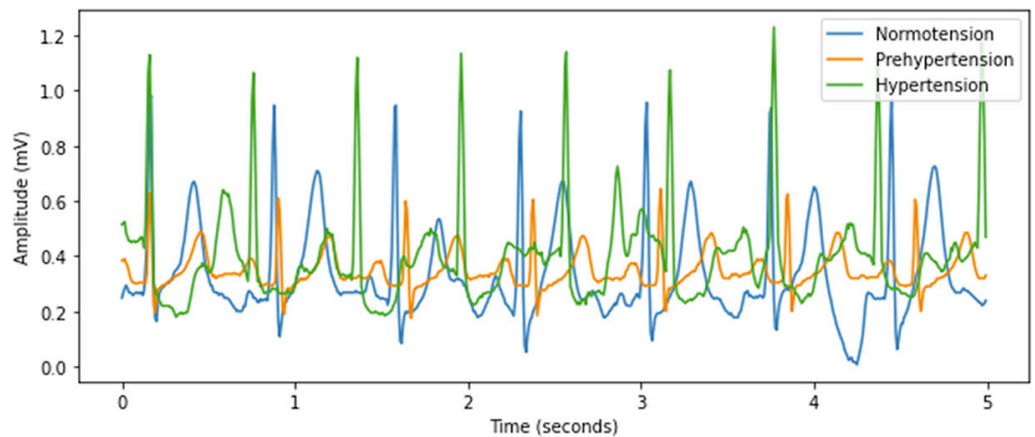
Fig. 2. ECG representations of three distinct classes: normotension, prehypertension, and hypertension
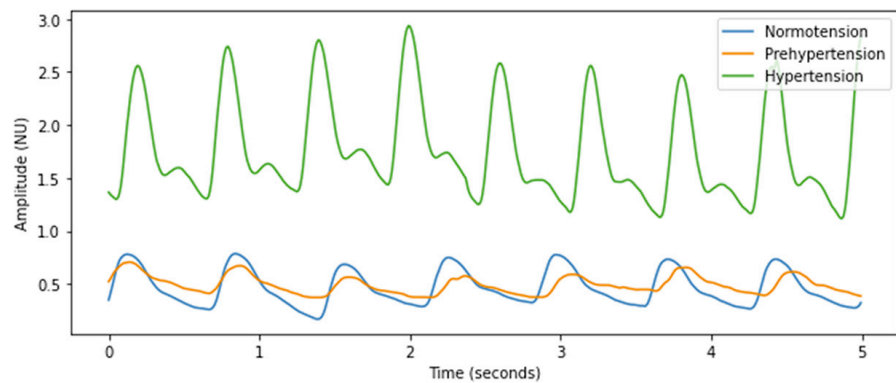
Fig. 3. PPG representations of three distinct classes: normotension, prehypertension, and hypertension

4.2 Identifying QRS-complex peaks in ECG

To detect QRS-complex peaks, the ECG signal was initially processed with a band-pass filter to highlight frequencies in the range of 5 to 20 Hz. This step effectively reduced interference caused by noise. Afterward, the filtered ECG signal was processed using the moving wave integration (MWI) technique, which utilized a Ricker (Mexican hat) wavelet. The squared integrated signal has been saved for further analysis. The outcomes of the MWI were carefully examined to determine if each local maximum corresponded to a QRS complex.

For a local maximum to be recognized as a QRS complex, it should not be mistaken for a T-wave. Furthermore, it needed to meet specific criteria: the peak had to exceed the predetermined QRS-complex detection threshold and appear after a refractory period of 0.2 seconds. Any local maximum that did not meet these criteria was classified as a noise peak. If a segment of the signal did not reveal a QRS complex, a backward search algorithm with a reduced threshold was used to improve the likelihood of identifying any missed QRS complexes. The approach for identifying QRS-complex peaks in an ECG is outlined in pseudocode in Algorithm 1.

Algorithm 1: Pseudocode for Identifying QRS-Complex Peaks in ECG

```
FUNCTION detectQRSComplex(ECG_Signal):

  // Apply a 5-20 Hz bandpass filter to the ECG signal
  filtered_signal = bandpassFilter(ECG_Signal,5Hz,20Hz)
  // Use MWI to process the signal.
  mwi_result = MWI(filtered_signal, wavelet="Ricker")
  // Square and store the integrated signal
    squared_signal = square(mwi_result)
    STORE squared_signal
    // Examine each local maximum
    FOR each local_maximum in squared_signal:
        // Check if the local maximum is a QRS-complex
        IF local_maximum NOT resembles T-wave AND
            local_maximum > QRS_threshold AND
            time_since_previous_peak > 0.2 seconds:
            MARK local_maximum as QRS-complex
        ELSE:
            MARK local_maximum as noise_peak
        // Backsearch for missed QRS-complexes
        IF no QRS-complex is detected in a specific span:
            backsearchAlgorithm(squared_signal, reduced_threshold)
END FUNCTION
```

All local peaks in the PPG signal were identified for PPG peak detection. A sample was identified as a PPG peak if it represented the highest value within a 30-sample range on both its left and right sides. When several consecutive samples had the same maximum value, the central sample was selected as the local peak.
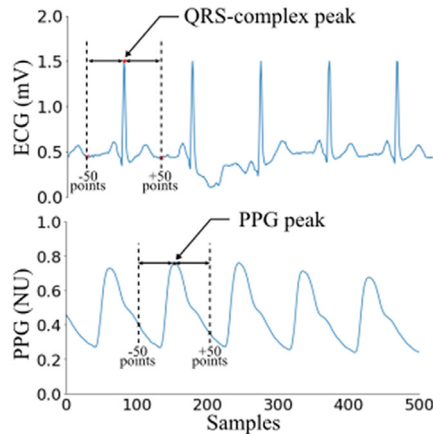
Fig. 4. Segments of ECG and PPG encompassing 50 data points on both the left and right sides of their respective peak values

After detecting the QRS-complex peaks and PPG peaks, 50 raw ECG samples before and after each QRS-complex peak and 50 raw PPG samples before and after each PPG peak were selected for further analysis. This selection is visually represented in Figure 4.
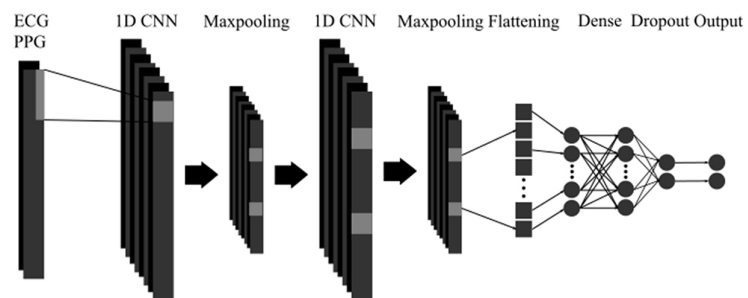
Fig. 5. Architecture of the CNN model

4.3 Design and structure of the CNN

Our CNN architecture, as shown in Figure 5, consisted of multiple layers. The architecture was initialized with a Conv1D layer, forming its foundation. This layer conducts a 1D convolution on the input data, using a specified number of filters (or kernels) to generate the output channels. The kernel size specifies the number of neighboring elements that a filter will evaluate concurrently. On the other hand, strides specify the progression that the filters take during convolution, subsequently affecting the output size. Post-convolution, the ReLu (rectified linear unit) activation function was used to introduce non-linearity to the output. The input shape defines the structure of the input data, indicating the time steps and features.

Next, the model integrated a MaxPooling1D layer to perform 1D max-pooling. By selecting the maximum value within each window of a predefined pool size, the spatial dimensions of the data were reduced. This step optimized computational efficiency and provided translational invariance to the input. Following this, the model introduced a second Conv1D layer, mirroring the first layer but with double the

number of filters. This layer enabled the model to extract more subtle features from the output of the previous layer.

After the second Conv1D layer, the model included a second MaxPooling1D layer, further reducing spatial dimensions in a manner similar to the previous layer. The sequence then shifted to the flatten layer, which transformed the 3D output of the preceding layer into a 1D vector, setting the stage for the subsequent fully connected (dense) layers. The dense layer, which accommodates 128 neurons, exemplifies a fully connected segment. Following the matrix multiplication, the ReLU activation function was applied. The dropout layer was also introduced as a regularization method that intermittently deactivates a portion of the input units during training. This mechanism mitigated overfitting and enhanced the model's adaptability.

The final dense layer, equipped with n output neurons, served as the primary fully connected layer, responsible for the ultimate classification. The softmax activation function translates the raw model output into probability scores, ensuring that their combined sum equals 1. The "mean squared error" (MSE) loss function was selected for model compilation, as it is the standard for regression tasks. The 'Adam' optimizer, known for its efficiency, was selected to refine the model's parameters during the training phase. Concurrently, additional evaluation metrics were measured, including a custom metric for determining the F1 score.

4.4 Data segregation for CNN training and evaluation

In CNN modeling, the way we segregated our dataset was crucial to ensuring model accuracy and generalization. For our CNN model, we carefully allocated our data resources. Specifically, 70% of the complete dataset was allocated for training. Within this segment, our model primarily learned the patterns and nuances of the data. However, training alone did not ensure an optimal model. It was crucial to validate the model's learning to ensure that it went beyond simply memorizing the data, which could result in overfitting. We further subdivided our training data to address this issue, setting aside 30% for validation. This validation subset served as a checkpoint, ensuring that our model's predictions were consistent and reliable throughout the training phase. Lastly, to assess the effectiveness and ability of our CNN model to generalize to new, previously unseen data, we set aside 30% of the entire dataset for testing. This testing phase provided insights into the real-world applicability and performance of our model. The strategic distribution of data not only facilitated a robust training environment but also ensured a comprehensive evaluation mechanism for our CNN model.

5 RESULTS

Our research thoroughly examined three specific input modalities to understand their role and effectiveness in hypertension when utilizing CNN. Firstly, we explored a combined approach by integrating ECG and PPG signals. This combination aims to leverage the complementary information from ECG and PPG, potentially enhancing the model's ability to recognize patterns related to HT. Secondly, we evaluated the ECG as a standalone input. Given the critical nature of ECG signals in capturing the heart's electrical activity, we were eager to understand their unique effectiveness in detecting HT, particularly when processed through a CNN. Finally, our study focused solely on the PPG signal. PPG, a non-invasive method for monitoring blood volume changes, added another dimension to our research. We aimed to determine the effectiveness of this single method for detecting HT using CNN. Across these varied modalities, we implemented various configurations and model architectures.

5.1   CNN configurations for hypertension detection with ECG and PPG signals

When ECG and PPG were used in combination, the F1 score consistently remained within a narrow range across various configurations (Table 1). This suggests that combining these inputs provides a more stable representation. In Trial B, the F1 scores fluctuated between 96.50% and 98.99%, indicating a synergistic effect where the combination of these inputs captured essential features for HT differentiation. The most effective configurations for this combined data often involved a stride of 2, particularly when using kernel sizes of 3 and 7. Filters of sizes 32 and 64 frequently yielded the highest scores. The highest F1 score, 98.99%, was achieved in Trial B using a filter of 64, a stride of 2, and a kernel size of 7.

Table 1. Performance of the proposed CNN-based hypertension detection using ECG and PPG inputs, presented in terms of F1 score

Trial	Filter	Stride = 2, Kernel = 3	Stride = 2, Kernel = 5	Stride = 2, Kernel = 7	Stride = 3, Kernel = 3	Stride = 3, Kernel = 5	Stride = 3, Kernel = 7
Trial A	8	91.70	91.96	90.48	90.15	90.54	90.60
Trial A	16	92.02	91.28	91.31	90.77	91.40	91.37
Trial A	32	92.35	92.20	91.76	90.68	90.98	91.90
Trial A	64	91.93	91.67	91.07	91.58	92.32	92.02
Trial B	8	98.41	98.20	98.20	96.50	97.48	98.23
Trial B	16	98.41	98.86	98.65	97.11	98.23	98.60
Trial B	32	98.89	98.65	98.68	98.15	98.31	98.44
Trial B	64	98.46	98.81	98.99	97.88	98.25	98.68
Trial C	8	94.82	94.44	94.34	92.74	93.01	94.44
Trial C	16	94.91	94.55	94.49	93.14	94.65	94.72
Trial C	32	95.27	94.66	95.10	94.15	94.28	94.66
Trial C	64	95.26	95.10	94.80	94.53	94.84	95.16

Table 2. Performance of the proposed CNN-based hypertension detection using ECG inputs, presented in terms of F1 score

Trial	Filter	Stride = 2, Kernel = 3	Stride = 2, Kernel = 5	Stride = 2, Kernel = 7	Stride = 3, Kernel = 3	Stride = 3, Kernel = 5	Stride = 3, Kernel = 7
Trial A	8	91.96	91.52	90.65	89.70	89.91	90.63
Trial A	16	91.82	91.07	91.04	89.76	91.79	90.30
Trial A	32	92.32	90.92	91.46	90.60	91.52	91.34
Trial A	64	91.22	91.67	90.95	90.18	90.95	91.58
Trial B	8	98.41	98.28	97.91	96.35	97.09	98.01
Trial B	16	97.56	98.20	98.31	97.35	97.64	97.80
Trial B	32	97.51	98.44	97.48	97.62	98.17	98.31
Trial B	64	97.51	98.17	98.25	97.88	98.09	98.54
Trial C	8	94.57	93.88	94.04	92.93	93.73	93.79
Trial C	16	94.82	93.96	94.02	93.35	93.33	94.02
Trial C	32	94.21	93.94	94.61	93.52	94.26	94.97
Trial C	64	94.44	93.98	93.73	93.69	94.30	94.26

5.2 CNN configurations for hypertension detection with ECG signals

Upon examining the F1 scores for ECG as a standalone input, specific configurations stood out (refer to Table 2). The configurations with a stride of 2 and a kernel of 7 in Trial B and a stride of 2 and a kernel of 3 in Trial C were notably effective. It hinted at the unique temporal and frequency features of the ECG. However, there was a significant variation in the F1 scores in Trial A, ranging from 89.70% to 92.32%. The study highlighted the sensitivity of ECG data to configuration changes and the potential benefits of using diverse kernel sizes. The highest F1 score, 98.99%, was achieved in Trial B using a filter of 64, a stride of 2, and a kernel size of 7.

5.3 CNN configurations for hypertension detection with PPG signals

When used alone, PPG data generally resulted in a lower F1 score, especially in Trial A, with scores as low as 77.53% (refer to Table 3). However, despite its limitations, PPG has shown significant potential in specific configurations. In Trial B, a stride of 2, a kernel of 3, and a filter of 64 yielded an F1 score of 95.63%. This result was competitive with some of ECG's top performances, demonstrating PPG's latent diagnostic potential when optimized. The most optimal performance for PPG-only input was achieved in Trial B, with an F1 score of 95.63% using a filter size of 64, a stride of 2, and a kernel size of 3.

Table 3. Performance of the proposed CNN-based hypertension detection using PPG inputs, presented in terms of F1 score

Trial	Filter	Stride = 2, Kernel = 3	Stride = 2, Kernel = 5	Stride = 2, Kernel = 7	Stride = 3, Kernel = 3	Stride = 3, Kernel = 5	Stride = 3, Kernel = 7
Trial A	8	84.20	83.90	84.52	77.53	81.16	79.91
Trial A	16	83.96	86.10	86.40	79.20	82.65	82.32
Trial A	32	86.01	86.90	86.10	82.26	84.26	86.37
Trial A	64	87.35	87.26	86.49	82.59	84.67	86.85
Trial B	8	92.98	93.51	93.35	85.83	88.06	89.00
Trial B	16	93.91	94.23	93.43	87.26	90.47	92.13
Trial B	32	95.26	95.50	95.02	90.12	93.78	93.72
Trial B	64	95.63	95.02	95.39	91.08	93.96	94.33
Trial C	8	90.38	91.14	90.76	85.08	86.57	88.34
Trial C	16	91.35	90.74	90.78	86.79	89.06	90.05
Trial C	32	90.57	91.16	91.73	87.82	89.63	91.50
Trial C	64	91.52	90.93	91.62	87.61	90.95	91.83

5.4 CNN configurations for hypertension detection with different input signals

As shown in Tables 1, 2, and 3, the study highlighted the effectiveness of the combined ECG and PPG input in the overall observations, demonstrating a high

F1 score and stability across configurations. While demonstrating sensitivity to configurations, the ECG showed high potential when properly adjusted. On the other hand, PPG, often considered a less significant factor, demonstrated its strengths in specific configurations, indicating its usefulness in specialized contexts. In summary, although the combined data produced the most reliable results, both ECG and PPG had their advantages and needed adjustments to maximize their F1 scores in detecting hypertension.

In terms of CNN configuration, the experimental results are presented as follows: The choice of stride, which determines the kernel's step size, revealed interesting insights. A smaller stride of 2, which generally captures finer details, resulted in higher F1 scores across the three input modalities: combined ECG and PPG, ECG alone, and PPG alone. This performance dominance was particularly evident with kernel sizes of 3 and 7. In contrast, a stride of 3, while competitive in some scenarios, such as with a filter size of 64, resulted in a drop in performance, particularly in PPG-only data for Trial A. It is suggested that a longer stride might sometimes overlook critical signal intricacies.

Kernel sizes provide an additional layer of analysis. The kernel's effectiveness in analyzing the input data varied depending on the size of the area being examined. The smallest size of 3 often achieved the highest scores, especially when combined with a stride of 2. This was most evident in ECG-only data, where it consistently outperformed other kernel sizes in Trials A and C. However, the medium-sized kernel of 5 delivered mixed results, excelling in certain configurations but being overshadowed in others. Interestingly, the largest kernel of 7 displayed erratic performance, excelling in specific configurations such as a stride of 2 and a filter of 32, but faltering in others.

The filter configurations enhanced the depth of the analysis. While the smallest filter size of 8 generally lagged, indicating potential limitations in capturing intricate PPG signals, intermediate sizes such as 16 and 32 often balanced computational efficiency with feature extraction. However, the standout performer consistently had the largest filter size of 64, especially prominent in the combined ECG and PPG data for Trial B.

The model demonstrated promising performance, as shown in Table 4, which displays the confusion matrix. It effectively differentiated individuals with HT (TP = 1939) from those without HT (TN = 1779). Nevertheless, there were instances of misclassifications, notably 19 false positives where individuals without HT were erroneously classified as having the condition and 21 false negatives where individuals with HT were inaccurately identified as not having the condition. Despite the model's commendable accuracy in identifying hypertensive and normotensive cases, reducing these misclassifications, particularly the false negatives, is crucial for enhancing the model's reliability in detecting non-cuff HT using ECG and PPG signals.

Table 4. Confusion matrix illustrating the detection performance using ECG and PPG signals

		Predicted	
		Normotension	Hypertension
TRUE	Normotension	1779 (TN)	19 (FN)
	Hypertension	21 (FP)	1939 (TP)

Notes: TP: true positive, TN: true negative, FP: false positive, FN: false negative.

5.5 Comparison of training loss across different CNN configurations

Figure 6 illustrates the training loss over 100 epochs for a CNN system developed for HT detection using ECG and PPG inputs. The system was assessed using different stride configurations, specifically a stride of 2 and a stride of 3, while maintaining the same kernel (kernel = 3) and filter (filter = 32) settings. During the training process, both configurations experienced a decrease in training losses. Starting with initial loss values of 0.2063 and 0.2150 for S = 2 and S = 3, respectively, both models showed improvement as epochs progressed.

Upon a more detailed inspection, the configuration with a stride of 2 consistently outperformed its counterpart. By the 100th epoch, the model with S = 2 achieved a training loss of 0.0211, while the model with S = 3 reached a loss of 0.0290. Throughout the training, there were slight fluctuations in the trajectory of the training loss for both configurations. However, the overall trend showed a consistent decrease in loss values, indicating successful optimization.
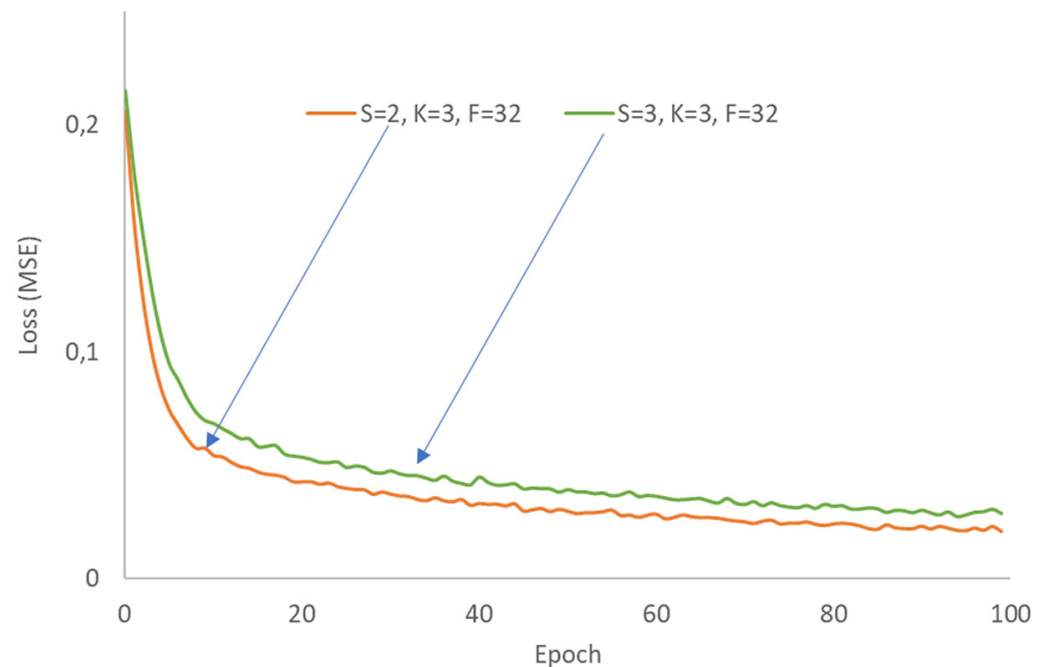
Fig. 6. Training loss trajectories over 100 epochs for CNN models developed for hypertension detection using ECG and PPG inputs, comparing different stride configurations (S = 2 and S = 3) while maintaining a consistent kernel (K = 3) and filter (F = 32)

While both configurations effectively reduced the training loss over time, the setup with S = 2, K = 3, and F = 32 demonstrated slightly better performance in minimizing the loss for this specific task. The findings emphasize the importance of choosing the right stride configuration to optimize CNN performance in detecting HT using ECG and PPG inputs.

Figure 7 displays the training loss of the CNN system for HT using ECG and PPG data. This figure shows the loss values over 100 training steps for various kernel setups. We examined CNNs with the same stride and filter but with different kernel sizes. The stride and filter were both set to 3 and 8. The training loss decreased over time for all configurations, indicating that the model improved during training.

The setup with a kernel size of 7 had the lowest training loss for most of the training steps. By the end of 100 steps, this configuration demonstrated the most favorable loss value of 0.0094, making it the optimal choice among the three configurations being considered. On the other hand, the configuration with a kernel size of 3 resulted in the highest training loss at step 100. Thus, when attempting to achieve the lowest training loss, the configuration with a kernel size of 7 was found to be the most effective for this particular task.
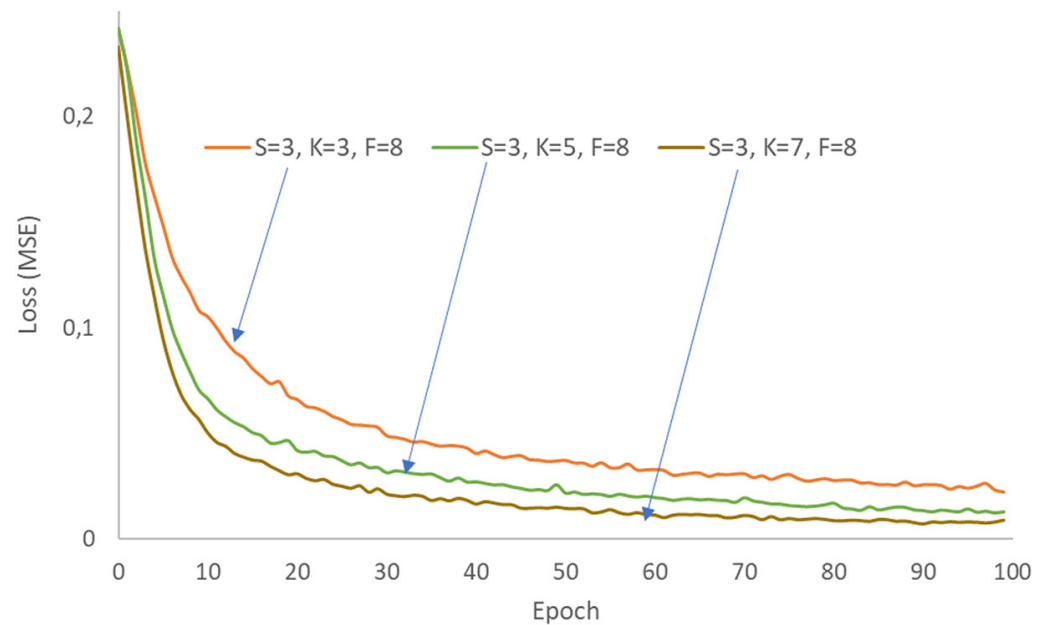
Fig. 7. Training loss trajectories over 100 epochs for CNN models developed for hypertension detection using ECG and PPG inputs, comparing different kernel configurations (K = 2, K = 5, and K = 7) while maintaining a consistent stride (S = 3) and filter (F = 8)

In the experimental results illustrated in Figure 8, CNN was trained using various filter sizes. The inputs to this CNN were ECG and PPG data. The training process was consistent across configurations in terms of stride (S = 2) and kernel (K = 7) size, varying only in the filter (F) size. For the configurations with filter sizes F = 8, F = 16, F = 32, and F = 64, the loss values at the beginning of the epochs were 0.2327, 0.2216, 0.2122, and 0.2053, respectively. By the 100th epoch, the losses had significantly decreased to 0.0068, 0.0027, 0.0039, and 0.0027, indicating effective learning across all configurations.

Upon analyzing the trend, it is evident that there was a decrease in the initial loss at the beginning of training as the filter size was increased. The configuration with a filter size of F = 64 showed the most rapid decrease in loss, reaching a value as low as 0.1316 by the second epoch, compared to F = 8, which decreased to 0.1964. It is suggested that larger filters facilitate faster convergence during the initial stages of training.

However, by the 100th epoch, the discrepancies in loss values among the configurations had became minimal, indicating that all configurations could achieve similar performance with adequate training time. The statement emphasizes the importance of considering computational efficiency and the potential risks of overfitting when choosing filter sizes, especially if minimal performance differences are noticed after extended training.
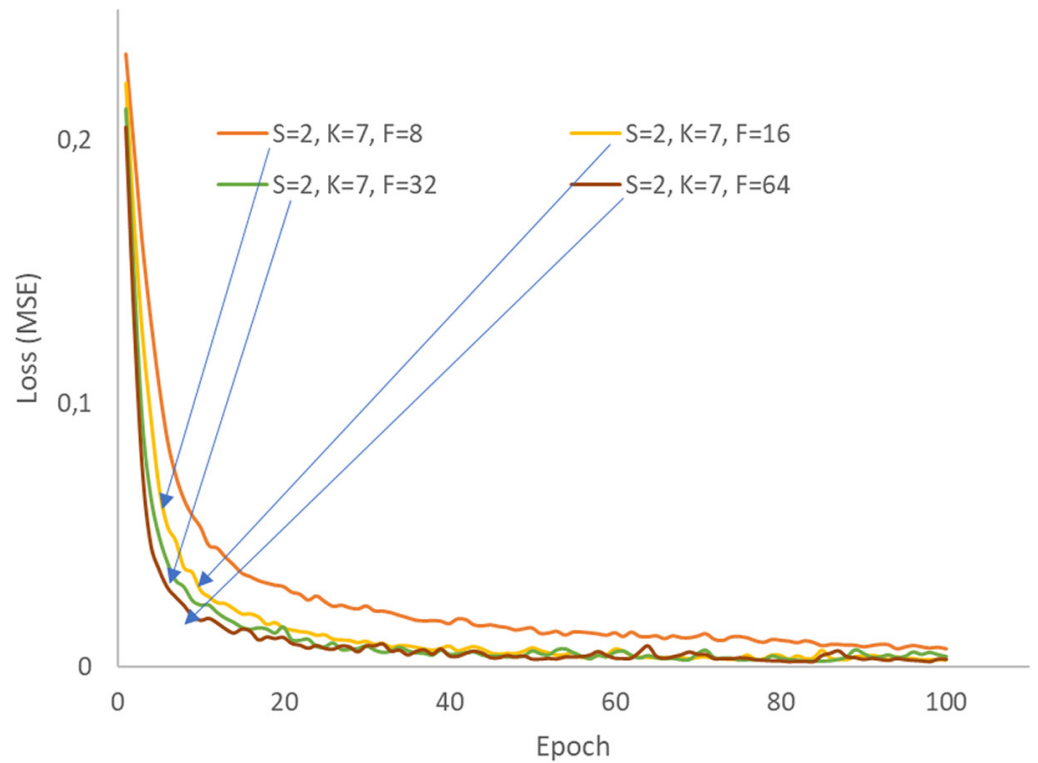
Fig. 8. Training loss trajectories over 100 epochs for CNN models developed for hypertension detection using ECG and PPG inputs, comparing different filter configurations (F = 8, F = 16, F = 32, and F = 64) while maintaining a consistent stride (S = 2) and kernel (K = 7)

5.6 Comparison of the proposed hypertension detection method with existing studies

To improve the detection of hypertension, we have introduced a new method and conducted a comprehensive comparison with established techniques. Table 5 provides a comprehensive comparison, encompassing input types, classifiers (machine learning and deep learning), and performance metrics. This framework helps us evaluate our method against other established approaches.

The field of hypertension detection research has seen a wide range of methodologies and features, each making a unique contribution to the accuracy of outcomes. The CNN used in the recent study demonstrated its exceptional capabilities when integrated with the combined ECG and PPG data. This integration resulted in impressive F1 scores of 92.35%, 98.99%, and 95.27% across three trials. These results emphasized CNN's ability to decipher intricate patterns, establishing its significance in detecting hypertension.

In a parallel development, Nuryani et al. introduced the swarm support vector machine (SSVM), which combines swarm optimization with the traditional SVM framework. When this method was applied to the pulse amplitude tonometry (PAT) and four-point pulse wave analysis (4 PPG) features, it achieved remarkable scores, notably 93.38% and 96.49% in specific trials. The combination of optimization strategies with traditional algorithms highlights their potential to enhance prediction results significantly.

Liang et al.'s range of classifiers, including LR and KNN, provided a varied perspective. Notably, the KNN classifier, when employed with certain features, achieved

an F1 score of 94.84%, reaffirming its effectiveness in detecting hypertension. Furthermore, the impact of deep learning extended beyond just CNNs. The integration of GoogleNet by Liang et al., particularly when combined with CWT scalograms, resulted in impressive scores in multiple trials. These results underscore the ability of deep learning models to extract patterns from visually detailed data.

When ECG and PPG data were analyzed using CNN, it produced unprecedented results and set a new standard for hypertension detection in terms of features. The findings above have highlighted the importance of comprehensively presenting data to achieve accurate detection. Concurrently, the consistent use of PAT and 4-point pulse pressure gradient (4 PPG) features across various studies, especially with the SVM, emphasized the significance of careful feature selection. The use of CWT (continuous wavelet transform) scalograms, in conjunction with models such as GoogleNet, has strengthened the argument for employing visual pattern recognition in studies related to hypertension. The approach by Martinez-Ríos et al., which integrated clinical metrics such as age and BMI with traditional classifiers such as SVM and KNN, presented a comprehensive perspective. Notably, an F1 score of 76.00% was achieved using SVM with 19 weighted set tiling (WST) features, demonstrating SVM's adaptability to diverse feature sets.

Table 5. Comparison of the proposed hypertension detection method with other studies

Trial	Features	Classifiers	F1 Score (%)
Trial-A	PAT and 10 PPG features	Logistic Regression by [28].	63.92
Trial-B	PAT and 10 PPG features	Logistic Regression by [28].	79.11
Trial-C	PAT and 10 PPG features	Logistic Regression by [28].	62.26
Trial-A	PAT and 10 PPG features	AdaBoost Tree by [28].	74.67
Trial-B	PAT and 10 PPG features	AdaBoost Tree by [28].	90.15
Trial-C	PAT and 10 PPG features	AdaBoost Tree by [28].	79.71
Trial-A	PAT and 10 PPG features	Bagged Tree by [28].	83.88
Trial-B	PAT and 10 PPG features	Bagged Tree by [28].	94.13
Trial-C	PAT and 10 PPG features	Bagged Tree by [28].	88.22
Trial-A	PAT and 10 PPG features	KNN by [28].	84.34
Trial-B	PAT and 10 PPG features	KNN by [28].	94.84
Trial-C	PAT and 10 PPG features	KNN by [28].	88.49
Trial-A	CWT Scalogram	The GoogleNet [29]	80.52
Trial-B	CWT Scalogram	The GoogleNet [29]	92.55
Trial-C	CWT Scalogram	The GoogleNet [29]	82.95
Trial-A	PAT and 4 PPG features	MLP [10]	90.71
Trial-B	PAT and 4 PPG features	MLP [10]	93.47
Trial-C	PAT and 4 PPG features	MLP [10]	87.54
Trial-A	PAT and 4 PPG features	SVM [10]	90.71
Trial-B	PAT and 4 PPG features	SVM [10]	94.58
Trial-C	PAT and 4 PPG features	SVM [10]	92.68

(Continued)

Table 5. Comparison of the proposed hypertension detection method with other studies *(Continued)*

Trial	Features	Classifiers	F1 Score (%)
Trial-A	PAT and 4 PPG features	SSVM [10]	93.38
Trial-B	PAT and 4 PPG features	SSVM [10]	96.49
Trial-C	PAT and 4 PPG features	SSVM [10]	93.76
Trial-A	19 WST Features	SVM [16]	76.00
Trial-A	Age, BMI, and Heart Rate	SVM [16]	69.57
Trial-A	Age, BMI, Heart Rate, plus 19 WST Features	KNN [19]	69.77
Trial-A	Age, BMI, Heart Rate, plus 19 WST Features	SVM [19]	72.34
Trial-A	ECG and PPG	CNN (This study)	92.35
Trial-B	ECG and PPG	CNN (This study)	98.99
Trial-C	ECG and PPG	CNN (This study)	95.27
Trial-A	ECG	CNN (This study)	92.32
Trial-B	ECG	CNN (This study)	98.54
Trial-C	ECG	CNN (This study)	94.97
Trial-A	PPG	CNN (This study)	87.35
Trial-B	PPG	CNN (This study)	95.63
Trial-C	PPG	CNN (This study)	91.83

In a comparative analysis of previous studies, it was observed that techniques such as CNN and SSVM produced significant results, but their effectiveness was highly dependent on the specific features they were associated with. The recent study by CNN achieved a zenith with an F1 score of 98.99% using ECG and PPG, demonstrating the synergy of advanced methodologies and optimized features. This interaction set the stage for future advancements in research on detecting hypertension.

6   DISCUSSION

Bio-signal inputs, such as ECG and PPG, have been extensively studied for HT detection [30]. Our experimental results, presented in three tables, provide insight into the comparative performances of these two modalities, both individually and in combination. Drawing on the theoretical background of ECG and PPG, this discussion aims to provide a deeper understanding of our findings and their implications in the broader context of HT research.

An ECG captures the heart's electrical activity over time, providing insights into the heart's rhythm and potential anomalies [31]. Conversely, PPG, an optically derived plethysmogram, is utilized to detect changes in blood volume within the microvascular tissue bed [32]. It operates by directing light into the skin and measuring the amount of light that is either transmitted or reflected to a sensor.

When considering the combined ECG and PPG input, our results unequivocally showed superior performance in detecting HT. The combination of these two inputs can be explained by understanding their inherent properties. While an ECG provides direct electrical information about heart activities and potential arrhythmias, a PPG offers complementary insights into blood flow and oxygenation. Fusing these

two data sources ensures a comprehensive view of cardiovascular health, thereby enhancing the model's predictive capabilities.

The individual analysis of an ECG demonstrated its effectiveness, particularly when properly calibrated. Given that the ECG directly measures the heart's electrical impulses, its sensitivity in detecting slight abnormalities often linked to HT becomes apparent. However, the results also suggested that the modality is sensitive to different configurations, highlighting the importance of optimal tuning.

On the other hand, PPG has historically been considered a secondary or supplementary modality in many cardiovascular studies. However, our findings illustrated that in specific configurations, PPG can indeed hold its ground. The nature of PPG, which captures blood volume changes and can indirectly infer heart rate and rhythm, offers a different perspective compared to ECG. PPG's utility can be maintained in specific scenarios, particularly when blood flow information becomes crucial.

Our study reaffirms the established understanding of the direct relevance of ECG in detecting cardiovascular health issues. At the same time, it elevates the status of PPG, emphasizing its unique contributions, particularly in specialized scenarios. The combination of ECG and PPG inputs in our model emphasizes the age-old adage in medical diagnostics: a comprehensive view derived from multiple data sources often yields the most accurate and actionable insights. Future studies could further explore the fusion techniques of these inputs to ensure that the information they provide is optimally utilized for even better HT detection outcomes.

Upon reviewing the experimental results, a more thorough examination of the CNN configurations provides valuable insights. CNN effectively utilizes the spatial hierarchies of input data by gradually condensing information through convolutional layers, pooling, and fully connected layers. This process preserves the spatial relationships and identifies complex patterns [33].

The tables presented emphasize the nuanced interplay between stride and kernel size in CNN configurations. The kernel size can be viewed as a window through which the network processes the input. A larger kernel enables the network to assimilate more contextual information at once, often resulting in the detection of larger patterns or features. Conversely, a smaller kernel size generally focuses on finer details [32]. In our experiment, we observed that varying kernel sizes resulted in different performance metrics. This demonstrates the impact of kernel dimensions on feature extraction, especially in biomedical signals such as ECG and PPG, which encompass both high-frequency and low-frequency information.

The tables presented in this study demonstrate that achieving an optimal F1 score depends on finding the right balance between stride and kernel size. This observation is consistent with previous scholarly works, which have shown that choosing the right combinations of stride and kernel for optimal performance depends on the characteristics [34]. Smaller filter sizes could be stacked to approximate the receptive field of a larger filter while using fewer parameters and enabling deeper architectures [35]. Our research supports this principle, particularly when examining the performance of configurations with smaller kernels arranged in deeper architectures.

Another crucial element was the depth, as indicated by the filter count. The depth of the CNN, determined by the number of filters, directly correlates with the model's capacity. By incorporating additional filters, the network is able to identify a greater number of features. However, this also increases computational demands and may lead to overfitting if not appropriately regularized. The trade-off between depth and overfitting was apparent, particularly when comparing configurations across different trials. Furthermore, building on a previous study [36] that introduced the concept of deep residual learning with ResNets, it was emphasized that deeper networks can achieve better performance. However, the use of residual connections

can make the training of very deep networks easier by addressing issues such as vanishing gradients.

In summary, while CNN's theoretical underpinnings provided a strong foundation, the results emphasized the importance of empirical tuning and exploration of configurations, particularly in biomedical signal processing. In future research, it may be beneficial to investigate architectures that can automatically adapt their configurations, such as neural architecture search (NAS), to optimally process input signals for the detection of hypertension.

In conclusion, while the present study and others emphasize the potential of methodologies such as CNN or SSVM, it is crucial to acknowledge the symbiotic relationship between these advanced algorithms and the features they utilize. Our recent study reached a pinnacle with an F1 score of 98.99% using CNN with ECG and PPG, showcasing the magic that occurs when cutting-edge techniques are paired with well-optimized features. It outlines a promising direction for our approach and provides a roadmap for future efforts in HT detection research.

7   LIMITATION

While paving the way for advanced non-cuff HT detection, our study has several limitations that need to be acknowledged. The dataset of ECG and PPG signals may not fully capture the physiological diversity across different populations. Factors such as age, ethnicity, and underlying comorbidities can introduce complexities in the signals, potentially influencing the results. Furthermore, the customized configurations of the CNN that we have developed, specifically optimized for our dataset, may not guarantee consistent performance when applied to other datasets or diverse patient demographics. The success of our model is closely linked to the quality of the ECG and PPG signals. Other medical conditions that could affect ECG and PPG signals were not thoroughly assessed, which could potentially act as confounding factors.

8   CONCLUSION

In our endeavor to propose innovative techniques for detecting HT, we thoroughly explored the potential of time-domain signals from ECG and PPG when processed through a one-dimensional CNN. Central to our findings was the observation that the combined use of both ECG and PPG signals significantly outperformed using each signal individually. The enhanced efficiency of ECG over PPG was particularly noteworthy. We achieved exemplary performance by directly applying these signals to CNNs and avoiding traditional extraction processes. Furthermore, our careful consideration of stride, kernel size, and filter optimization highlights their importance in effectively configuring a high-performing CNN for HT detection. Our experiments resulted in an impressive F1 score of 98.99% when we combined ECG and PPG signals using the optimized CNN configuration, representing a significant advancement in cuffless HT diagnostics. These results suggest that utilizing deep learning tools with ECG and PPG inputs can significantly enhance medical diagnostics. Nevertheless, while our findings show promise, they were obtained under controlled conditions and may face challenges when applied to real-world scenarios. The implications of this research are far-reaching, suggesting a broader impact beyond the scope of HT and indicating a promising future for diagnostic methods that do not necessitate the use of cuffs. In this era of technological advancement, we plan to expand our methodologies to cover various medical domains, improve our models, and engage in real-time monitoring.

9   FUTURE STUDY

Drawing upon our recent research on HT detection using combined ECG and PPG with CNNs, we have identified several promising avenues for future exploration. Firstly, our findings have highlightened the effectiveness of CNNs in biomedical signal processing. However, there is potential to enhance CNN configurations through hyperparameter tuning, architectural adjustments, and exploration of various activation functions to achieve superior outcomes. Additionally, building on the success of ECG and PPG integration, the incorporation of other biomedical signals, such as electroencephalogram (EEG), could further enhance the data, offering a comprehensive perspective that could improve detection accuracy.

10   ACKNOWLEDGMENT

11   REFERENCES

[1]   B. Fishman *et al.*, "Adolescent hypertension is associated with stroke in young adulthood: A nationwide cohort of 1.9 million adolescents," *Stroke*, vol. 54, no. 6, pp. 1531–1537, 2023. https://doi.org/10.1161/STROKEAHA.122.042100

[2]   O. Abdelbagi, I. R. Musa, S. M. Musa, S. A. ALtigani, and I. Adam, "Prevalence and associated factors of hypertension among adults with diabetes mellitus in northern Sudan: A cross-sectional study," *BMC Cardiovascular Disorders*, vol. 21, pp. 1–7, 2021. https://doi.org/10.1186/s12872-021-01983-x

[3]   S. S. Chugh *et al.*, "Epidemiology of sudden cardiac death: Clinical and research implications," *Progress in Cardiovascular Diseases*, vol. 51, no. 3, pp. 213–228, 2008. https://doi.org/10.1016/j.pcad.2008.06.003

[4]   S. I. Putri, A. Widiyanto, J. T. Atmojo, and A. S. Fajriah, "Early detection of hypertension as an effort to prevent disease complications," *Jurnal Empathy Pengabdian Kepada Masyarakat*, pp. 115–123, 2021. https://doi.org/10.37341/jurnalempathy.v0i0.55

[5]   D. L. Joyce, "The invisible silent killer," in *Mayo Clinic Proceedings*, 2021, vol. 96, no. 8, pp. 2022–2024. https://doi.org/10.1016/j.mayocp.2021.06.015

[6]   N. Pratiwi, S. Hidayat, W. Ardiatna, A. Hidayat, and I. Supono, "New insight of the implication blood pressure detection differences using aneroid sphygmomanometer and digital blood pressure on medical examination," in *Journal of Physics: Conference Series*, 2020, vol. 1528, no. 1, p. 012057. https://doi.org/10.1088/1742-6596/1528/1/012057

[7]   A. V. Chobanian *et al.*, "Seventh report of the joint national committee on prevention, detection, evaluation, and treatment of high blood pressure," *Hypertension*, vol. 42, no. 6, pp. 1206–1252, 2003. https://doi.org/10.1161/01.HYP.0000107251.49515.c2

[8]   F. Beltman, W. Heesen, A. Smit, J. May, K. Lie, and B. Meyboom-de Jong, "Acceptance and side effects of ambulatory blood pressure monitoring: Evaluation of a new technology," *Journal of Human Hypertension*, vol. 10, pp. S39–42, 1996.

[9]   D. Shimbo, M. Abdalla, L. Falzon, R. R. Townsend, and P. Muntner, "Role of ambulatory and home blood pressure monitoring in clinical practice: A narrative review," *Annals of Internal Medicine*, vol. 163, no. 9, pp. 691–700, 2015. https://doi.org/10.7326/M15-1270

[10] N. Nuryani, T. P. Utomo, N. Wiyono, A. D. Sutomo, and S. Ling, "Cuffless hypertension detection using swarm support vector machine utilizing photoplethysmogram and electrocardiogram," *Journal of Biomedical Physics and Engineering*, vol. 13, no. 5, pp. 477–488, 2023. https://doi.org/10.31661/jbpe.v0i0.2206-1504

[11] S. Gupta, A. Singh, A. Sharma, and R. K. Tripathy, "Higher order derivative-based integrated model for cuff-less blood pressure estimation and stratification using PPG signals," *IEEE Sensors Journal*, vol. 22, no. 22, pp. 22030–22039, 2022. https://doi.org/10.1109/JSEN.2022.3211993

[12] S. Montagna *et al.*, "Machine learning in hypertension detection: A study on World Hypertension Day data," *Journal of Medical Systems*, vol. 47, no. 1, p. 1, 2022. https://doi.org/10.1007/s10916-022-01900-5

[13] P. Jain, P. Gajbhiye, R. Tripathy, and U. R. Acharya, "A two-stage deep CNN architecture for the classification of low-risk and high-risk hypertension classes using multi-lead ECG signals," *Informatics in Medicine Unlocked*, vol. 21, p. 100479, 2020. https://doi.org/10.1016/j.imu.2020.100479

[14] J. S. Rajput, M. Sharma, T. S. Kumar, and U. R. Acharya, "Automated detection of hypertension using continuous wavelet transform and a deep neural network with Ballistocardiography signals," *International Journal of Environmental Research and Public Health*, vol. 19, no. 7, p. 4014, 2022. https://doi.org/10.3390/ijerph19074014

[15] F. López-Martínez, E. R. Núñez-Valdez, R. G. Crespo, and V. García-Díaz, "An artificial neural network approach for predicting hypertension using NHANES data," *Scientific Reports*, vol. 10, no. 1, p. 10620, 2020. https://doi.org/10.1038/s41598-020-67640-z

[16] H. A. Abu-Alsaad, "CNN-based smart parking system," *International Journal of Interactive Mobile Technologies*, vol. 17, no. 11, pp. 155–170, 2023. https://doi.org/10.3991/ijim.v17i11.37033

[17] B. Al-Rami, K. M. A. Alheeti, W. M. Aldosari, S. M. Alshahrani, and S. M. Al-Abrez, "A new classification method for drone-based crops in smart farming," *International Journal of Interactive Mobile Technologies*, vol. 16, no. 9, pp. 164–174, 2022. https://doi.org/10.3991/ijim.v16i09.30037

[18] S. T. Ahmed and S. M. Kadhem, "Using machine learning via deep learning algorithms to diagnose the lung disease based on chest imaging: A survey," *International Journal of Interactive Mobile Technologies*, vol. 15, no. 16, pp. 95–112, 2021. https://doi.org/10.3991/ijim.v15i16.24191

[19] E. Martinez-Ríos, L. Montesinos, and M. Alfaro-Ponce, "A machine learning approach for hypertension detection based on photoplethysmography and clinical data," *Computers in Biology and Medicine*, vol. 145, p. 105479, 2022. https://doi.org/10.1016/j.compbiomed.2022.105479

[20] E. Martinez-Ríos, L. Montesinos, M. Alfaro-Ponce, and L. Pecchia, "A review of machine learning in hypertension detection and blood pressure estimation based on clinical and physiological data," *Biomedical Signal Processing and Control*, vol. 68, p. 102813, 2021. https://doi.org/10.1016/j.bspc.2021.102813

[21] R. T. H. Promi, R. A. Nazri, M. S. Salim, and S. T. U. Raju, "A deep learning approach for non-invasive hypertension classification from PPG signal," in *2023 International Conference on Next-Generation Computing, IoT and Machine Learning (NCIM)*, 2023, pp. 1–5. https://doi.org/10.1109/NCIM59001.2023.10212940

[22] G. J. Hassing *et al.*, "Blood pressure-related electrocardiographic findings in healthy young individuals," *Blood Pressure*, vol. 29, no. 2, pp. 113–122, 2020. https://doi.org/10.1080/08037051.2019.1673149

[23] Z. Marcinkevics, M. Greve, J. I. Aivars, R. Erts, and A. H. Zehtabi, "Relationship between arterial pressure and pulse wave velocity using photoplethysmography during the post-exercise recovery period," *Acta Univesitatis Latviensis: Biology*, vol. 753, pp. 59–68, 2009.

[24] L.-P. Yao and W.-Z. Liu, "Hypertension assessment based on feature extraction using a photoplethysmography signal and its derivatives," *Physiological Measurement*, vol. 42, no. 6, p. 065001, 2021. https://doi.org/10.1088/1361-6579/aba537

[25] M. Saeed *et al.*, "Multiparameter intelligent monitoring in intensive care II: A public-access intensive care unit database," (in eng), *Crit. Care. Med.*, vol. 39, no. 5, pp. 952–960, 2011. https://doi.org/10.1097/CCM.0b013e31820a92c6

[26] A. L. Goldberger *et al.*, "PhysioBank, PhysioToolkit, and PhysioNet: Components of a new research resource for complex physiologic signals," *Circulation*, vol. 101, no. 23, pp. e215–e220, 2000. https://doi.org/10.1161/01.CIR.101.23.e215

[27] A. V. Chobanian *et al.*, "The seventh report of the joint national committee on prevention, detection, evaluation, and treatment of high blood pressure: The JNC 7 report," *Jama*, vol. 289, no. 19, pp. 2560–2571, 2003. https://doi.org/10.1001/jama.289.19.2560

[28] Y. Liang, Z. Chen, R. Ward, and M. Elgendi, "Hypertension assessment via ECG and PPG signals: An evaluation using MIMIC database," *Diagnostics*, vol. 8, no. 3, p. 65, 2018. https://doi.org/10.3390/diagnostics8030065

[29] Y. Liang, Z. Chen, R. Ward, and M. Elgendi, "Photoplethysmography and deep learning: Enhancing hypertension risk stratification," *Biosensors*, vol. 8, no. 4, p. 101, 2018. https://doi.org/10.3390/bios8040101

[30] M. Sharma, J. S. Rajput, R. S. Tan, and U. R. Acharya, "Automated detection of hypertension using physiological signals: A review," *International Journal of Environmental Research and Public Health*, vol. 18, no. 11, p. 5838, 2021. https://doi.org/10.3390/ijerph18115838

[31] Z. Bouzid, S. S. Al-Zaiti, R. Bond, and E. Sejdić, "Remote and wearable ECG devices with diagnostic abilities in adults: A state-of-the-science scoping review," *Heart Rhythm*, vol. 19, no. 7, pp. 1192–1201, 2022. https://doi.org/10.1016/j.hrthm.2022.02.030

[32] J. Allen, D. Zheng, P. A. Kyriacou, and M. Elgendi, "Photoplethysmography (PPG): State-of-the-art methods and applications," *Physiological Measurement*, vol. 42, no. 10, p. 100301, 2021. https://doi.org/10.1088/1361-6579/ac2d82

[33] P. Rajesh, A. Murugan, B. Murugamantham, and S. Ganesh, "Lung cancer diagnosis and treatment using AI and Mobile applications," *International Journal of Interactive Mobile Technologies (iJIM)*, vol. 14, no. 17, pp. 189–203, 2020. https://doi.org/10.3991/ijim.v14i17.16607

[34] J. T. Springenberg, A. Dosovitskiy, T. Brox, and M. Riedmiller, "Striving for simplicity: The all convolutional net," *arXiv preprint arXiv:1412.6806*, 2014.

[35] A. Krizhevsky, I. Sutskever, and G. E. Hinton, "Imagenet classification with deep convolutional neural networks," *Advances in Neural Information Processing Systems*, vol. 25, 2012.

[36] K. He, X. Zhang, S. Ren, and J. Sun, "Deep residual learning for image recognition," in *Proceedings of the IEEE conference on computer vision and pattern recognition*, 2016, pp. 770–778. https://doi.org/10.1109/CVPR.2016.90

12   AUTHORS

Nuryani Nuryani is a Professor of Medical Instrumentation in the Department of Physics at the University of Sebelas Maret. His research interests include artificial intelligence in biomedical engineering (E-mail: nuryani@mipa.uns.ac.id).

Trio Pambudi Utomo is affiliated with the Department of Physics, University of Sebelas Maret. His research interests include intelligent medical instrumentation.

Nurhasan Agung Prabowo is affiliated with the Faculty of Medicine, University of Sebelas Maret. His research interests include internal medicine, rheumatology, and immunology.

Aripriharta is affiliated with the Department of Electrical Engineering, Universitas Negeri Malang, Indonesia. His research interests include low-power electronics converters for Biomedical IoT/Wearable devices.

Muhammad Yazid is affiliated with the Department of Biomedical Engineering, Institut Teknologi Sepuluh Nopember, Indonesia. His research interests include bio-medical signals processing.

Mohtar Yunianto is affiliated with the Department of Physics, University of Sebelas Maret. His research interests include physics theory and computation.